2D Pseudo-Homogeneous Simulation Model of an Additively Manufactured Reactor for Catalytic Methanation

Supplementary Material to the Article: Utilization of Synthetic Steel Gases in an Additively Manufactured Reactor for Catalytic Methanation

Alexander Hauser*, Jürgen Karl

Chair of Energy Process Engineering, Friedrich-Alexander-Universität Erlangen-Nürnberg, Fürther Straße 244f, 90429 Nürnberg, Germany
* Corresponding author; alexander.hauser@fau.de

S.1. Aim of the simulation model

The simulation model described below was developed to validate and quantify the trends observed in the experimental investigations with ADDmeth1 with respect to the reactors' catalytic ignition behavior. In particular, consistent, practical operating maps for estimating the minimum and maximum permissible reaction channel inlet temperatures for stable and safe reactor operation in steady-state are to be determined for the syngas power range and reactant gas mixtures also investigated experimentally. Transient effects are not taken into account.

The simulation model was implemented in COMSOL Multiphysics® 6.0 (COMSOL Inc., Stockholm, Sweden). The following sections describe the implemented modules, approximations and boundary conditions.

S.2. Simulation model and boundary conditions

S.2.1. Geometry

Based on the additively manufactured reactor ADDmeth1 presented in [1], only its main innovation, the conically widening reaction channel, was simulated for simplicity (see Figure S1). The catalyst volume is represented here as a porous matrix. Furthermore, the thermowell present in the real case for measuring axial temperature profiles is not simulated. Instead, its area/volume is taken into account by reducing the reaction channel diameter (D_{inlet} = 7.42 mm, D_{outlet} = 31.86 mm). The reaction channel length of 167 mm is identical. Deviating from the real design, in the simulation the gas flows in and out via the end faces (see Figure S1), which avoids numerical problems and significantly reduces the calculation time compared to a lateral in- and outlet.

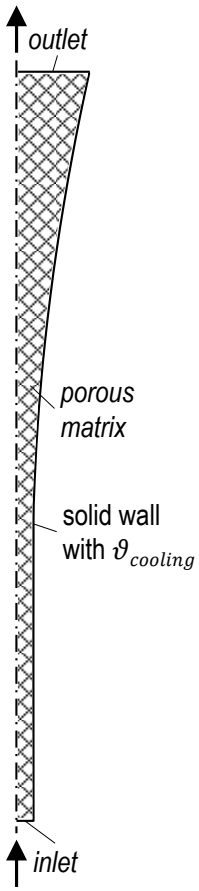

Figure S1. Rotationally symmetric simulation geometry of the reaction channel of ADDmeth1.

S.2.2. *Material data*

S.2.2.1. *Thermodynamic system of the gas phase*

The internal COMSOL® database provides material data for all required fluids (CO_2, CO, H_2, CH_4, N_2, H_2O). By defining a thermodynamic system of the mentioned components based on the ideal gas law, relevant mixture variables are also calculated (including feedback of the other simulation modules). The default settings for the property models were retained.

S.2.2.2. *Material data of the solid phase*

The solid phase of the catalyst bed assumed to be porous material must be defined manually. For the heat capacity at constant pressure and the thermal conductivity of the solid (Ni/Al_2O_3), the temperature-dependent functions according to Liu et al. [2] are used. An extrapolation of the values beyond the validity range described in [2] is not performed; here, the last value of the validity range in each case is assumed to be constant for higher/lower temperatures. The solid density is assumed to be 1987 kg/m³ according to Neubert et al. [3], who used the same catalyst. Also according to [3], a (constant) porosity of the catalyst bed/porous material of ε_{bed} = 0.4 is used; boundary effects are neglected. This experimentally determined value is in very good agreement with the value calculated for the inlet cross section according to the empirical model of Pushnov [4] (cylindrical pellets, d = 1.9 mm).

S.2.3. *Chemistry*

The *'Chemistry'* module implements the involved chemical reactions. The thermodynamic system described above provides the required thermodynamic quantities of the involved species. Both the CO methanation and the WGS reaction are implemented as reversible reactions. The direct input possibility of the module for equilibrium constant, Arrhenius expression and rate constants is not used, because this information is already included in the (separate) calculation of the reaction rate.

The kinetic approach of Rönsch et al. [5] is taken to implement the intrinsic reaction kinetics, which was used before in combination with the given catalyst [6]. The kinetics were developed for a Ni/Al_2O_3 catalyst with a similar high nickel content (~50%) and verified for a relatively large temperature and pressure range (275-360 °C, 1-5 bar) [5]. This describes the methanation reaction system on the basis of the above reactions; the CO_2 methanation is taken into account by the linear combination of these two. The aforementioned approach follows a Langmuir-Hinshelwood-Hougen-Watson (LHHW) approach. The rate coefficients are calculated according to the Arrhenius approach and the adsorption constants according to the van't Hoff approach. The equilibrium constants are calculated according to Elnashaie and Elshishini [7].

When moving to catalyst pellets with dimensions in the millimeter range, as also used in ADDmeth1, mass transport limitations increase and the reaction rate declines compared to the intrinsic reaction rate. To account for the influence of diffusion processes, effective reaction rates $r_{eff,n}$ can be calculated as the product of the intrinsic reaction rate and effectiveness factors for pore diffusion $\eta_{pore,n}$ and external mass transport, or film diffusion respectively, $\eta_{ext,n}$ (Equation (S1)).

$$r_{eff,n} = r_{int,n} \cdot \eta_{pore,n} \cdot \eta_{ext,n} \tag{S1}$$

According to Jess and Wasserscheid [8], the pore efficiency can be calculated as a function of the Thiele modulus using Equation (S2) (valid for all catalyst geometries). The Thiele modulus relates the reaction rate at surface conditions to the mass transport by pore diffusion. It can be calculated for an irreversible first order reaction and for any catalyst geometry according to Equation (S3) [9]:

$$\eta_{pore,n} = \frac{\tanh(\Phi_\mathrm{n})}{\Phi_\mathrm{n}} \tag{S2}$$

$$\Phi_n = \frac{V_p}{A_{p,ext}} \cdot \sqrt{\frac{k_{V,n} \cdot \rho_p}{D_{eff,CO}}} \tag{S3}$$

V_p and $A_{p,ext}$ denoted the geometric particle volume and surface area of a catalyst pellet, respectively, $k_{V,n}$ the volume-specific rate constants of the respective reaction n, ρ_p the density of the catalyst particle, and $D_{eff,CO}$ the effective diffusion rate of CO in the catalyst pores.

The factor $\eta_{ext,n}$, describing the inhibition by film diffusion, depends on the mass transfer coefficient β, the geometric mass-related catalyst surface $A_{mass,ext}$, and the internal mass transfer described above (Equation (S4)) [8]:

$$\eta_{ext,n} = \frac{\beta \cdot A_{mass,ext}}{\beta \cdot A_{mass,ext} + \eta_{pore,n} \cdot k_{V,n}} \tag{S4}$$

After the implementation according to the system described above, initial simulation runs showed that the numerical ignition behavior of the catalytic reactions deviated significantly from that observed experimentally.

Steeper gradients and significantly higher maximum temperatures were observed in experiments. A similar behavior was also noticed by Gruber [10,11], who stated as possible causes an overestimation of the thermal conductivity of the perfused fixed-bed (too high heat dissipation) and/or an underestimation of the effective reaction rate. The latter may again be due to the selection of the intrinsic reaction rate or the calculation of mass transfer limitations. The challenging aspect of this problem is that the parameters r_{int}, η_{pore}, and η_{ext}, which determine the effective reaction rate, depend on each other and consequently cannot be considered individually.

Gruber [10,11] approaches this problem by an elaborate iterative analysis of these three factors. He performs modifications which are as justified as possible and which can be reconciled with constraints from the literature. Finally, he achieves a very high agreement between numerical simulation and experimental results by means of adjustments of the intrinsic reaction rate (modification of activation energy, pre-exponential factor and adsorption coefficient of water), the internal mass transfer limitation (modification of the Thiele modulus) and the external mass transfer limitation (empirical correlation of the Sherwood number).

Since the obtained correlations are not directly transferable (e.g. dependence on used intrinsic kinetics and catalyst geometry) and fitting by the method used by Gruber would be disproportionately time consuming for the actual simulation objective (see Section S.1.), an additional factor ξ is used in this work to modify the effective reaction rates (Equation (S5). ξ is composed of the composition specific sub-factors ξ_{BFG} and ξ_{BOFG} (Equation (S6)), weighted according to the BFG:BOFG ratio ($x_{BFG} = 1$: 100% BFG, $x_{BFG} = 0$: 100% BOFG).

$$r_{eff,n} = r_{int,n} \cdot \eta_{pore,n} \cdot \eta_{ext,n} \cdot \xi \tag{S5}$$

$$\xi = x_{BFG} \cdot \xi_{BFG} + (1 - x_{BFG}) \cdot \xi_{BOFG} \tag{S6}$$

ξ_{BFG} and ξ_{BOFG} in turn are linearly dependent on the inlet standard flow rate according to Equations (S7) and (S8). The definition of the curves is based on iteratively determined values for ξ_{BFG} and ξ_{BOFG} at the lowest and highest syngas power investigated (OP1.1/OP1.5 and OP2.1/OP2.5, respectively), at which the hotspot temperature coincides with that of the experiments.

$$\xi_{BFG} = -0.6789 \cdot \dot{V}_{N,0} \left[\frac{\text{min}}{\text{l}}\right] + 19.844 \tag{S7}$$

$$\xi_{BOFG} = -0.3975 \cdot \dot{V}_{N,0} \left[\frac{\text{min}}{\text{l}}\right] + 26.484 \tag{S8}$$

This approach limits the validity of the simulation model to the syngas power range considered and to the reactant gas mixtures used. In addition, a loss of information is to be expected, since the numerical adaptation via a global factor ξ is considerably more undifferentiated than, for example, the adaptation according to Gruber [10,11] (several adapted factors). Detailed statements about the three-dimensional temperature field off the hotspot are not possible.

Furthermore, the implemented thermal conductivity (see Section S.2.5.) was assumed to be applicable. Any deviations of this parameter are therefore also contained in ξ and its dependencies.

The dependence of ξ on the volume flow rate could be due to an implicit temperature dependence. As observed experimentally, the overall temperature level increases (with otherwise unchanged conditions) with increasing reactant flow rate. Gruber made the same observation and also concluded that the temperature influence on the intrinsic kinetics was overestimated (activation energy too high), which has an effect especially at lower volume flow rates with lower temperatures [10]. Consequently, a higher elevation of the effective reaction rate would be necessary at lower volume flows, which in turn results in larger values for ξ. The fact that

a second correlation, dependent on the BFG:BOFG ratio, appears to exist could be related to the fact that the relative relationship between heat release and heat transport (primarily convective) changes with the reactivity of the reactant gas. Another issue could be that the chosen kinetics and its underlying assumed reaction mechanism describe the mixed CO/CO_2 methanation inadequately (not taking into account competitive adsorption of CO and CO_2), which may lead to inconsistencies in kinetic and thermodynamic parameters [12,13].

S.2.4. *Fluid flow*

To model the flow through the porous medium, the Brinkman equations (module *'Brinkman Equations'*) are used, whose mathematical model is an extension of Darcy's law by including a term to account for viscous transport. Thus, continuity equation and momentum balance are taken into account and pressure and velocity vector are considered as independent variables. [14]

A compressible fluid was assumed under steady-state conditions, neglecting additional forces (swirl, gravity, inertial term, Forchheimer/Ergun drag). The no-slip condition applies to solid walls. The permeability of the porous medium was calculated by the Kozeny-Carman equation using the volume equivalent diameter of the cylindrical pellets as the particle diameter.

The presented assumptions are applicable in laminar flow conditions. However, the simulations performed showed that these are not always fulfilled, but are often in the transitional regime. For the operating points discussed, the Reynolds numbers were in the range of 450 – 525.

S.2.5. *Heat transfer*

The used module *'Heat Transfer in Porous Media'* solves the heat equation by assuming local thermal equilibrium between solid and fluid phase. Both convection and heat conduction in the porous material are considered. The only relevant volumetric heat source Q is the released heat of reaction. This is calculated in the *'Chemistry'* module. It is assumed that the heat of reaction is only released in the pore volume of the porous material.

The model according to Zehner/Bauer/Schlünder is used to calculate the effective thermal conductivity of the catalyst bed (VDI Wärmeatlas [15], module D6.3). The primary and the secondary influencing parameters are taken into account.

The inlet temperature into the reaction channel ϑ_{in} and its influence on the ignition behavior of the reactor is the main subject of the simulative investigation. Accordingly, the parameter ϑ_{in} is varied.

In the real application of the ADDmeth concept, the heat of reaction is transferred via the reaction channel wall to the internal reactant gas preheating or to the heat dissipation system. For simplicity, a spatially constant wall temperature $\vartheta_{cooling}$ is assumed in the simulation model. This is linked to ϑ_{in} via an empirical function obtained from the ADDmeth1 experimental data (see Equation (S9)). By means of a case differentiation at the relevant root of the quadratic function, it is ensured that $\vartheta_{cooling}$ does not become smaller than ϑ_{in}. This corresponds to the real case. In addition, extrapolation beyond the data range of the empirical function is not permissible.

$$T_{cooling} = \begin{cases} T_{in}, & T_{in} < 458.7\ \mathrm{K} \\ T_{in} + \left(-0.0031\, T_{in}^2 \left[\frac{1}{\mathrm{K}^2}\right] + 3.4286\, T_{in} \left[\frac{1}{\mathrm{K}}\right] - 920.42\right) [\mathrm{K}], & 458.7\ \mathrm{K} \leq T_{in} \leq 552\ \mathrm{K} \end{cases} \tag{S9}$$

S.2.6. *Chemical species transport*

The transport of the chemical species is modeled in the module *'Transport of Concentrated Species'*. In the mass balance, diffusive and convective mass transport phenomena are considered. Additionally, a rate expression describing the components production or consumption is included.

The mixture-averaged diffusion model is used, where the binary diffusion coefficients are calculated in the *'Chemistry'* module based on the kinetic gas theory [16]. Migration in an electric field is not applicable and Knudsen and thermal diffusion are neglected.

S.2.7. *Mesh and numerical issues*

The mesh used for numerical calculation is of tetragonal shape and follows the contour of the reaction channel ('mapped' mesh). In the region of parallel reaction channel walls, the cells have a rectangular shape; with increasing expansion, distortion occurs. Accordingly, the mesh segments also increase in the r-direction with increasing reaction channel diameter. At the transition to the solid wall, the mesh is refined by means of boundary layers. The mesh, comprising a total of 17,000 elements, achieves a very high average quality with a value of 0.9539 (min. quality: 0.6267).

Solving the simulation model, which has a total of 157,816 degrees of freedom, is not trivial. In order to support the solver, in a first step only the flow field is simulated in steady-state and in a second step a solution of the overall system of equations is found by means of a time-dependent simulation. This solution serves as a set of initial values for the subsequent steady-state simulations for parameter investigation.

References

1. Hauser, A.; Neubert, M.; Feldner, A.; Horn, A.; Grimm, F.; Karl, J. Design and Implementation of an Additively Manufactured Reactor Concept for the Catalytic Methanation. *Appl. Sci.* **2022**, *12*, 9393, doi:10.3390/app12189393.
2. Liu, D.M.; Tuan, W.H.; Chiu, C.C. Thermal Diffusivity, Heat Capacity and Thermal Conductivity in Al2O3Ni Composite. *Mater. Sci. Eng. B* **1995**, *31*, 287–291, doi:10.1016/0921-5107(94)01163-X.
3. Neubert, M.; Hauser, A.; Pourhossein, B.; Dillig, M.; Karl, J. Experimental Evaluation of a Heat Pipe Cooled Structured Reactor as Part of a Two-Stage Catalytic Methanation Process in Power-to-Gas Applications. *Appl. Energy* **2018**, *229*, 289–298, doi:10.1016/j.apenergy.2018.08.002.
4. Pushnov, A.S. Calculation of Average Bed Porosity. *Chem. Pet. Eng.* **2006**, *42*, 14–17, doi:10.1007/s10556-006-0045-x.
5. Rönsch, S.; Köchermann, J.; Schneider, J.; Matthischke, S. Global Reaction Kinetics of CO and CO2 Methanation for Dynamic Process Modeling. *Chem. Eng. Technol.* **2016**, *39*, 208–218, doi:10.1002/ceat.201500327.
6. Neubert, M.; Widzgowski, J.; Rönsch, S.; Treiber, P.; Dillig, M.; Karl, J. Simulation-Based Evaluation of a Two-Stage Small-Scale Methanation Unit for Decentralized Applications. *Energy and Fuels* **2017**, *31*, 2076–2086, doi:10.1021/acs.energyfuels.6b02793.
7. Elnashaie, S.S.E.H. and Elshishini, S.S. *Modelling, Simulation and Optimization of Industrial Fixed Bed Catalytic Reactors. Topics in Chemical Engineering, Volume 7*; Gordon and Breach Science Publishers, 1993; ISBN 2-88124-883-7.
8. Jess, A.; Wasserscheid, P. *Chemical Technology - An Integral Textbook*; Wiley-VCH: Weinheim, 2013; ISBN 978-3-527-30446-2.
9. Levenspiel, O. *Chemical Reaction Engineering*; Wiley, 1999; ISBN 978-0-471-25424-9.
10. Gruber, M. Detaillierte Untersuchung Des Wärme- Und Stofftransports in Einem Festbett-Methanisierungsreaktor Für Power-to-Gas Anwendungen, Karlsruher Institut für Technologie (KIT), Karlsruhe, Germany, 2019.
11. Gruber, M.; Wiedmann, D.; Haas, M.; Harth, S.; Loukou, A.; Trimis, D. Insights into the Catalytic CO2

Methanation of a Boiling Water Cooled Fixed-Bed Reactor: Simulation-Based Analysis. *Chem. Eng. J.* **2021**, *406*, 126788, doi:10.1016/j.cej.2020.126788.

12. Burger, T.; Donaubauer, P.; Hinrichsen, O. On the Kinetics of the Co-Methanation of CO and CO2 on a Co-Precipitated Ni-Al Catalyst. *"Applied Catal. B, Environ.* **2020**, 119408, doi:10.1016/j.apcatb.2020.119408.
13. Schmider, D.; Maier, L.; Deutschmann, O. Reaction Kinetics of CO and CO2 Methanation over Nickel. *Ind. Eng. Chem. Res.* **2021**, *60*, 5792-5805. doi:10.1021/acs.iecr.1c00389.
14. COMSOL Inc. CFD Module User's Guide. Available online: https://doc.comsol.com/6.0/docserver/#!/com.comsol.help.cfd/html_CFDModuleManual.html (accessed on 13 October 2022).
15. Verein deutscher Ingenieure *VDI-Wärmeatlas*; VDI e.V., Ed.; 11th ed.; Springer: Berlin, Heidelberg, 2013; ISBN 978-3-642-19980-6.
16. COMSOL Inc. Chemical Reaction Engineering User's Guide. Available online: https://doc.comsol.com/6.0/docserver/#!/com.comsol.help.chem/html_ChemicalReactionEngineeringModuleManual.html (accessed on 13 October 2022).